Supplementary Material

Acetic Acid Vapours Adsorption-Induced Morphological Change in FeBTC Metal–Organic Frameworks

Davide Tocco,[a] David Chelazzi,[a] Andrea Salis,[b,] Emiliano Fratini,[a,]* Andrea Casini,[a] Rosangela Mastrangelo[a]*

[a] Department of Chemistry ‘‘Ugo Schiff” & CSGI, University of Florence, via della Lastruccia 3, Sesto Fiorentino (FI) I-50019, Italy.

[b] Department of Chemical and Geological Sciences & CSGI, University of Cagliari, SS 554 bivio Sestu, 09042 Monserrato (CA), Italy

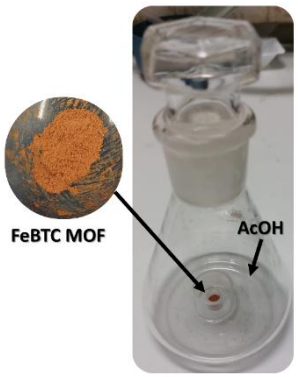

Figure S1. Schematic representation of FeBTC system for acetic acid adsorption.

Kinetic Models

Pseudo-first-order model (PFO)

The pseudo-first-order kinetic equation, most commonly expressed in the form proposed by Ho and McKay,[1] is:

$$ln\, ln\left[q_e - q(t)\right] = lnq_e - k_1 t \qquad \text{(S1)}$$

where q is the amount of adsorbed solute, q_e its value at equilibrium, k_1 is the pseudo-first order rate constant, and t is the time.

The experimental data were fitted using the alternative expression:

$$q(t) = q_e\,[1 - exp\,(-k_1 t)\,] \qquad \text{(S2)}$$

The pseudo-first-order kinetic equation differs in principle from a true first order equation in two aspects:

The equilibrium adsorption capacity (q_e) may deviate from the theoretical maximum surface capacity, since real adsorbents are typically heterogeneous and the contributions of transport phenomena and chemical reactions are experimentally inseparable. As a result, the parameter $k_1(q_e - q_t)$ does not directly quantify the number of available sites, in contrast to a true first-order formulation.

The coefficient of the exponential term $exp(-k_1 t)$ can be adjusted to values greater than 1, whereas in a true first-order equation it must remain strictly equal to 1.

Pseudo-second-order model (PSO)

According to the pseudo-second-order model, the adsorption rate is proportional to the number of available adsorbent sites, and the kinetic expression is generally employed in the form introduced by Ho and McKay:[1]

$$\frac{t}{q(t)} = \frac{t}{q_e} + \frac{1}{k_2 {q_e}^2} \qquad \text{(S3)}$$

where k_2 is the pseudo-second-order kinetic rate constant. q_e can, in principle, differ from the theoretical maximum adsorption capacity of the surface (see above), thus the model equation differs from a true second order equation.

To obtain statistically relevant comparisons with the other models, the following expression that considers the original scale (y = q(t)) was used:

$$q(t) = q_e \frac{k_2^* t}{1 + k_2^* t} \qquad \text{(S4)}$$

where $k^*_2 = k_2 q_e$.

$$q(t) = q_e\,[1 - exp\,(-k_1 t)\,] \quad \text{(S5)}$$

$$q(t) = q_e\,\frac{k_2^* t}{1+k_2^* t} \quad \text{(S6)}$$

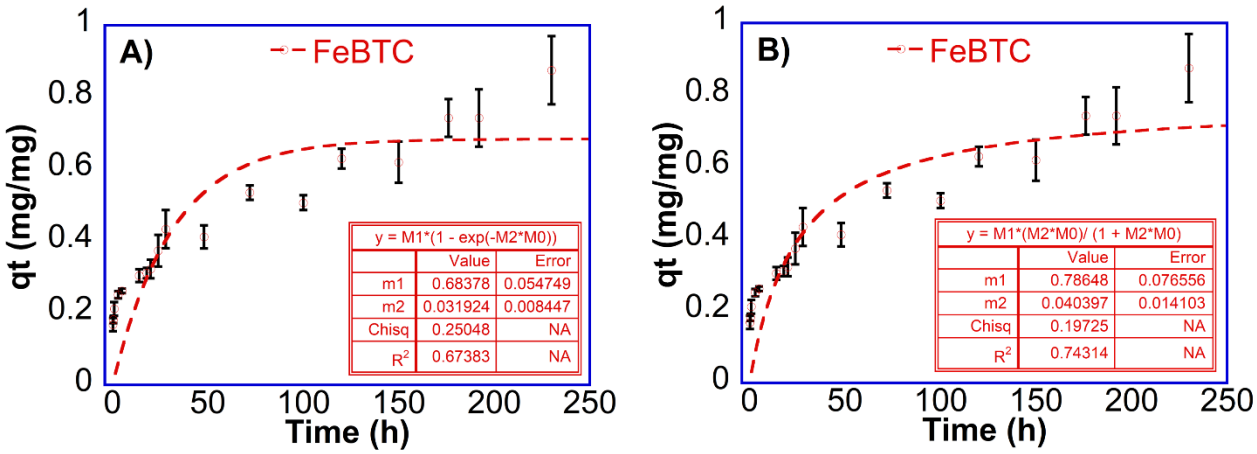

Figure S2. Adsorption of AcOH by FeBTC under saturated atmosphere of AcOH at 23°C, fitted to the **A)** PFO and **B)** PSO model.

Double exponential model (DE)

DE is an empirical model that is not based on any assumption regarding the chemistry of the process but rather describes sorption from a mathematical point of view.

The model uses a double exponential function to correlate the two-step kinetics of the adsorption of a metal ion onto a matrix:

$$q(t) = q_e - \frac{D1}{m} exp\,(-K_{D1} t) - \frac{D2}{m} exp\,(-K_{D2} t) \quad \text{(S7)}$$

where D1 and D2 are sorption rate parameters (mmol L^{-1}) of the rapid and the slow step, respectively, and KD1 and KD2 are parameters (min^{-1}) controlling the mechanism; m is the adsorbent amount in the solution (g L^{-1}). If the exponential term corresponding to the rapid process is assumed to be

negligible on the overall kinetics (KD1>>KD2), the model equation can be simplified to a single exponential (SE):

$$q(t) = q_e - \frac{D1}{m} exp\,(-K_{D1}t) \qquad \text{(S8)}$$

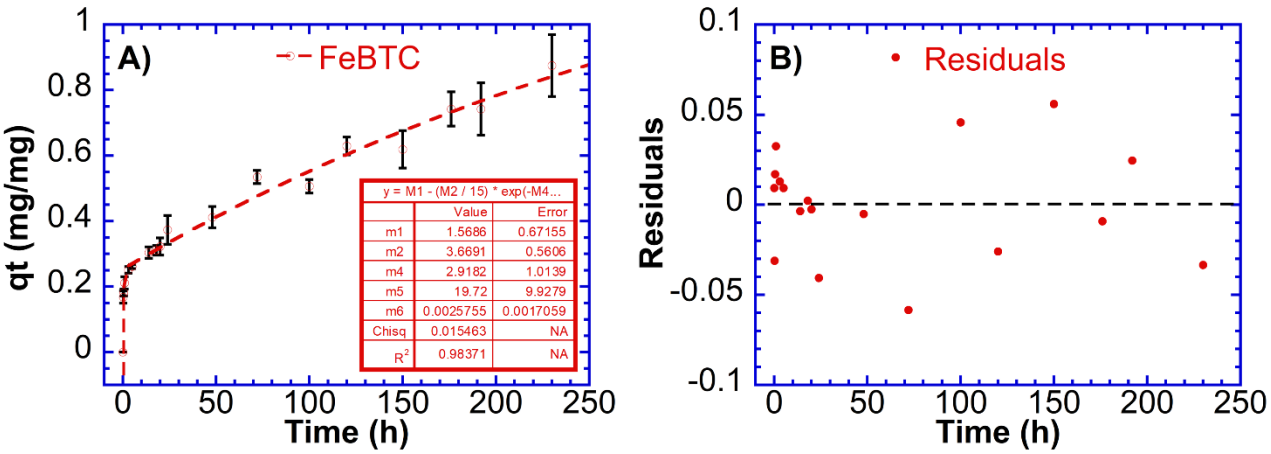

Figure S3. A) Adsorption of AcOH by FeBTC under saturated atmosphere of AcOH at 23°C, fitted to the DE model, **B)** Residuals graph relative to DE model.

Calculation of FeBTC surface area from SAXS data

The values of $I \times Q^4$ registered at the high-Q plateau, in the Porod plot (Fig. 4 A in the main text), were used to calculate the S/V variation with respect to the 0 h samples. Considering the equation reported by Spalla *et al.*[2] for inner-pores and inter-grain porosity (the samples being powders in air):

$$\frac{S}{V}[mm^{-1}] = \frac{(I_{high-Q} \times Q^4)}{2\pi \cdot SLD^2} \qquad \text{(S9)}$$

where SLD is the X-ray scattering length density of the material. When the sample's thickness, the powder packing factor and material density are known, the specific surface area can be obtained by dividing the calculated S/V by the material density. In the present case, being these factors unknown, we calculated the relative S/V variation (%) with respect to the initial S/V value, i.e. the S/V calculated for the pristine sample (0 h):

Supplementary Material

$$\frac{S}{V}\ Rel.Variation\ (\%) = \frac{S/V_{Sample} - S/V_{0\,h}}{S/V_{0\,h}} = \left(\frac{\frac{(I\times Q^4)_{Q=0.05,Sample}}{2\pi\cdot SLD^2_{FeBTC+AcOH}} - \frac{(I\times Q^4)_{Q=0.05,0\,h}}{2\pi\cdot SLD^2_{FeBTC}}}{\frac{(I\times Q^4)_{Q=0.05,0\,h}}{2\pi\cdot SLD^2_{FeBTC}}} \right) \times 100 \qquad \text{(S10)}$$

where SLD_{FeBTC} was calculated considering the empirical value of density reported by Sapnik et al.[3] and $SLD_{FeBTC + AcOH}$ values were obtained considering the volume fraction of the adsorbed acetic acid.

SAXS/USAXS characterization of FeBTC

SAXS curves acquired on 0 h – 237 h samples in the 0.005 – 0.66 $Å^{-1}$ range were modeled according to the following equation, accounting for a Porod slope at low-Q and Gaussian-shaped bumps at high-Q, after subtracting data's background:

$$I(Q) = \frac{A}{Q^n} + B \cdot exp\left[-\frac{(Q-Q_1)^2}{2{\sigma_1}^2}\right] + C \cdot exp\left[-\frac{(Q-Q_2)^2}{2{\sigma_2}^2}\right] + D \cdot exp\left[-\frac{(Q-Q_3)^2}{2{\sigma_3}^2}\right] \qquad \text{(S11)}$$

where A, B, C and D are scale parameters, n is the Porod exponent, while Q_1, Q_2, Q_3 are the centers and σ_1, σ_2, σ_3 the full widths half maximum of the Gaussian peaks.

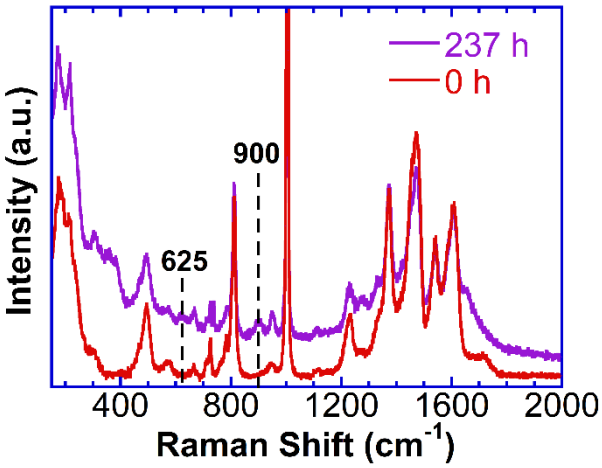

Figure S4. Raman spectrum of FeBTC and FeBTC exposed to AcOH vapours (237 h) (wavenumber range from 150 to 2000 cm^{-1}).

Supplementary Material

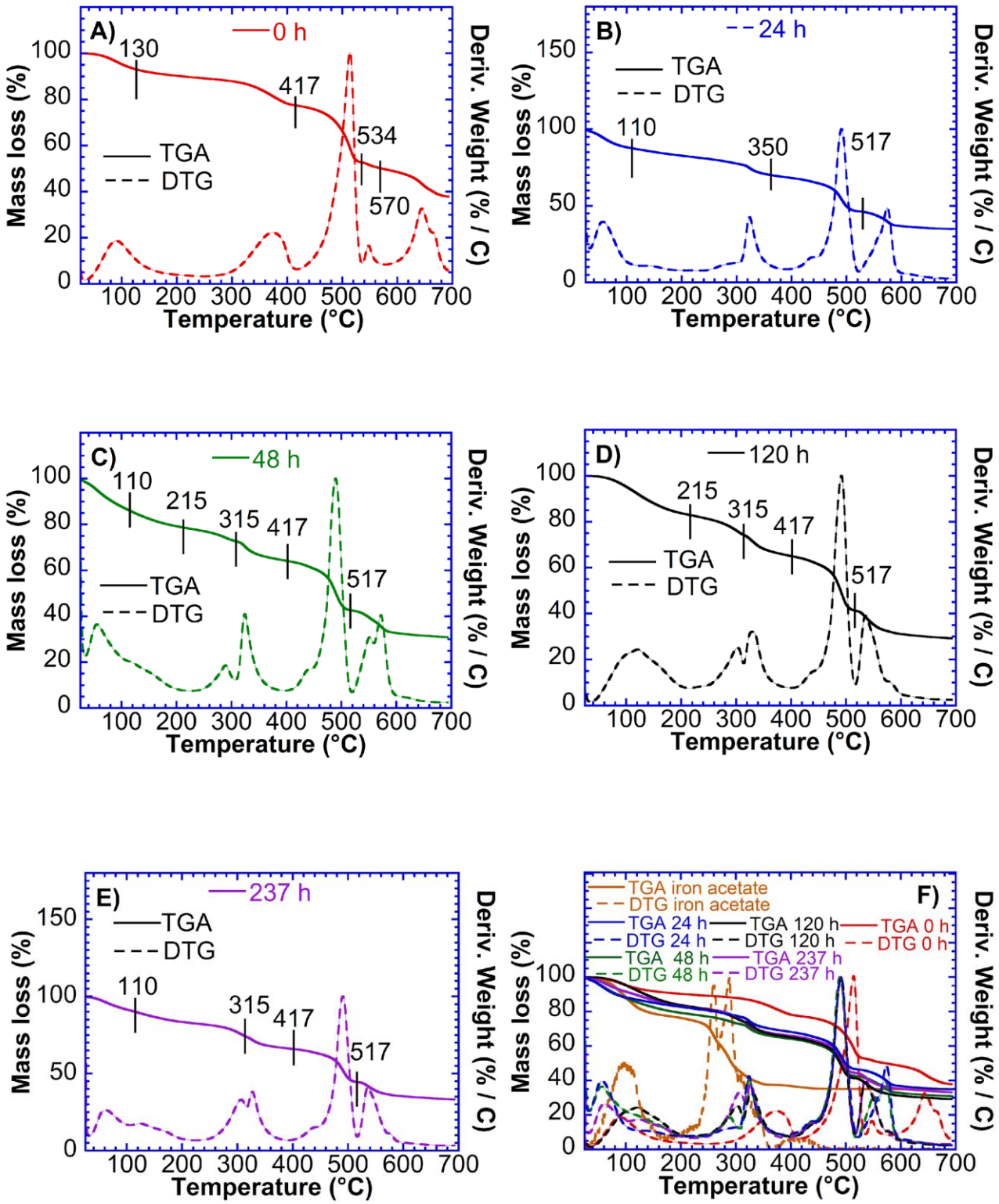

Figure S5. Thermogravimetric (TGA) and derivative thermogravimetric (DTG) profiles of FeBTC samples exposed to AcOH vapours for different exposure times (A–E): 0, 24, 48, 120 and 237 h. Panel F shows the overlay of all TGA and DTG curves together with iron acetate for comparison.

Supplementary Material

Table S1: Mass loss (%) of FeBTC samples exposed to AcOH vapours for different times (0 h, 24 h, 48 h, 120 h, and 237 h)

Sample	Mass loss (%) 30°C <T < 130 °C	Mass loss (%) 130°C < T < 417 °C	Mass loss (%) 417 °C < T < 534	Mass loss (%) 534 °C < T < 570	Mass loss (%) T > 570 °C
Fe-BTC	6.75	14.53	22.94	2.71	11.52

	Mass loss (%) 30°C <T < 110 °C	Mass loss (%) 110°C < T <350	Mass loss (%) 350 °C < T < 517	Mass loss (%) T >517°C
24 h	11.44	20.26	21.13	11.29

	Mass loss (%) 30°C <T < 110 °C	Mass loss (%) 110°C < T <215	Mass loss (%) 215 °C < T < 315	Mass loss (%) 315 °C < T < 417	Mass loss (%) 417 °C < T < 517	Mass loss (%) T > 517
48 h	14.9	8.58	6.9	9.4	21.12	12.33
120		17 (from 30°C to 215°C)	8.17	9.94	22.88	12.1
237 h	8.55	7.34	8.36	8.42	19.67	10.76

Supplementary Material

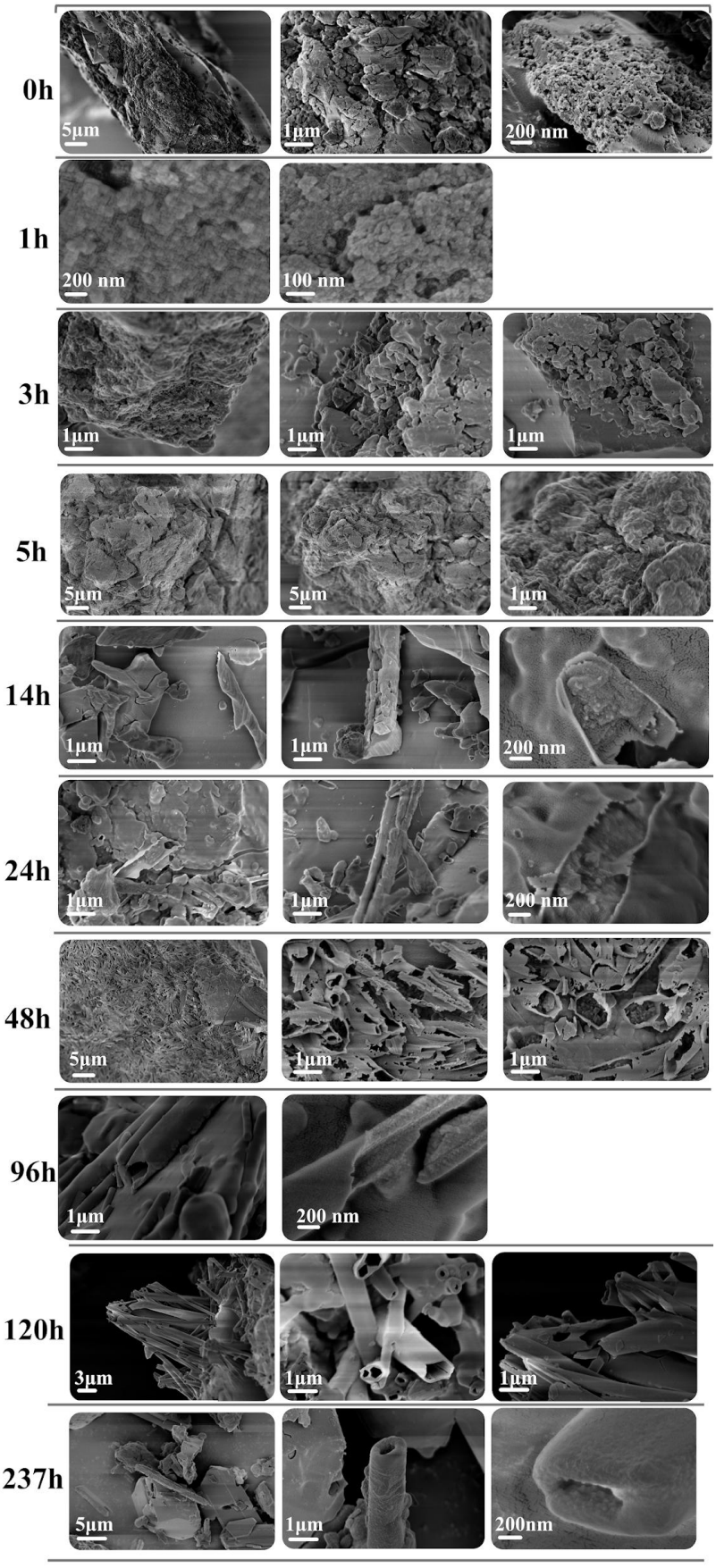

Figure S6. SEM images of FeBTC exposed to AcOH over a time range from 0 to 237 h.

Supplementary Material

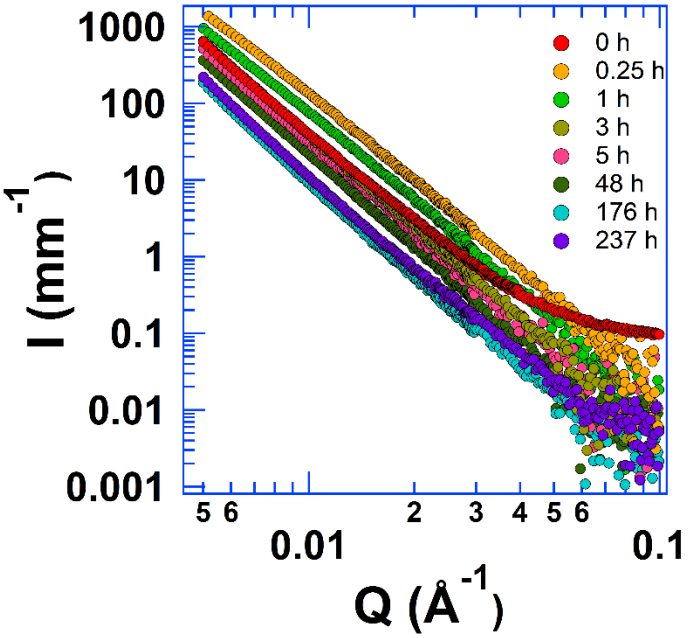

Figure S7. SAXS curves in the 0.05 – 0.1 Å-1 range, from which the Porod plot shown in Fig. 4 A (main text) was obtained.

Table S2. Fitting parameters of the three Gaussian functions used to fit the high-Q bumps shown in fig. 4 C (main text). The periodicity Q_1, ~2xQ_1, ~3xQ_1 is evident.

Time (h)	B (Scale)x 10^{-3}	$Q_{peak,1}$ (Å^{-1})	σ_1	C (Scale)x 10^{-3}	$Q_{peak,2}$ (Å^{-1})	σ_2	D (Scale)x 10^{-3}	$Q_{peak,3}$ (Å^{-1})	σ_3
0	90 ± 1	0.14 ± 0.01	0.06 ± 0.01	50 ± 1	0.29 ± 0.01	0.04 ± 0.01	3.0 ± 0.5	0.49 ± 0.01	0.05 ± 0.01
3	4.0 ± 0.5	0.14 ± 0.01	0.05 ± 0.01	3.5 ± 0.5	0.29 ± 0.01	0.05 ± 0.01	3.0 ± 0.5	0.48 ± 0.01	0.04 ± 0.01
48	6.0 ± 0.5	0.14 ± 0.01	0.05 ± 0.01	4.5 ± 0.5	0.30 ± 0.01	0.05 ± 0.01	3.0 ± 0.5	0.47 ± 0.01	0.04 ± 0.01
120	20 ± 1	0.14 ± 0.01	0.05 ± 0.01	15 ± 1	0.29 ± 0.01	0.06 ± 0.01	8.0 ± 0.5	0.47 ± 0.01	0.04 ± 0.01
237	10 ± 1	0.14 ± 0.01	0.05 ± 0.01	12 ± 1	0.28 ± 0.01	0.06 ± 0.01	6.0 ± 0.5	0.48 ± 0.01	0.05 ± 0.01

References

1 Y. Ho and G. McKay, *Process Biochem.*, 1999, **34**, 451–465.

2 O. Spalla, S. Lyonnard and F. Testard, *J. Appl. Crystallogr.*, 2003, **36**, 338–347.

3 A. F. Sapnik, I. Bechis, S. M. Collins, D. N. Johnstone, G. Divitini, A. J. Smith, P. A. Chater, M. A. Addicoat, T. Johnson, D. A. Keen, K. E. Jelfs and T. D. Bennett, *Nat. Commun.*, 2021, **12**, 2062.